Computers and Mathematics with Applications 75 (2018) 3903–3917

Contents lists available at ScienceDirect

Computers and Mathematics with Applications

journal homepage: www.elsevier.com/locate/camwa

On an equivalent representation of the Green's function for the Helmholtz problem in a non-absorbing impedance half-plane

S. Rojas [a,b,*], R. Hein [c], M. Durán [c]

[a] Department of Applied Geology, Western Australian School of Mines, Curtin University, Kent Street, Bentley, Perth, WA 6102, Australia
[b] Escuela de Ingeniería, Pontificia Universidad Católica de Chile, Av. Vicuña Mackenna 4860, Macul, Santiago, Chile
[c] INGMAT R&D Centre, José Miguel de la Barra 412, 4to piso, Santiago, Chile

ARTICLE INFO

Article history:
Received 17 August 2017
Received in revised form 1 February 2018
Accepted 1 March 2018
Available online 15 March 2018

Keywords:
Green's function
Helmholtz problem
Impedance boundary condition
Non-absorbing half-plane
Surface waves

ABSTRACT

The Green's function associated with the Helmholtz problem in a non-absorbing impedance half-plane can be expressed as an integral form. In the non-absorbing case, the presence of surface waves presents a challenge in order to obtain accurate approximations. In this work, we present an equivalent representation for this Green's function, expressed as a sum of analytical terms and bounded integrals. The resulting representation is numerically stable and it can be estimated by any well known robust integration rule for bounded intervals. We provide a detailed description of the equivalent representation and we validate it with numerical experimentation.

1. Introduction

Several problems in engineering can be modeled as the scattering of an incident acoustic field due to a local perturbation of a half-plane. One such problem is, for instance, the determination of electromagnetic modes of two-dimensional photonic crystals, where the photonic crystal is assumed to be covered by a substrate which is modeled as a half-plane [1,2]. Another situation where this problem appears is in the computation of harbor resonances in marine hydraulics, where the sea is assumed to fill a locally perturbed half-plane and the perturbation is given by the harbor geometry [3–5]. Another example is the propagation of elastic wave modes above the ground due to blasting and drilling operations in a mine. Here, the mine can be considered to be the local perturbation of a half-plane [6].

When considering a time-harmonic decomposition for acoustic waves, i.e., an explicit time dependency of the form $e^{-i\omega t}$, with ω denoting the angular frequency, the problem of acoustic sound propagation above ground can be reduced to the estimation of a spatial total field $u_T(\mathbf{x})$ (decomposed into a known incident field plus an unknown scattered field), satisfying the following impedance (or Robin) boundary condition (over the boundary of the locally perturbed half-plane):

$$\partial_n u_T(\mathbf{x}) = i\beta\kappa\, u_T(\mathbf{x}), \tag{1}$$

where ∂_n denotes the partial derivative in the normal direction (that is assumed to be outwardly directed), $\beta \in \mathbb{C}$ denotes the acoustic admittance of the boundary and $\kappa = \omega/c > 0$ is the wave number (with c being the sound speed). When the

* Corresponding author at: Department of Applied Geology, Western Australian School of Mines, Curtin University, Kent Street, Bentley, Perth, WA 6102, Australia.
E-mail addresses: srojash@gmail.com (S. Rojas), ricardo.hein@ingmat.com (R. Hein), mario.duran@ingmat.com (M. Durán).

https://doi.org/10.1016/j.camwa.2018.03.001
0898-1221/

real part of the admittance constant is positive, the boundary has an absorbing-energy property, implying that the scattered field has the standard Sommerfeld acoustic behavior as $|\mathbf{x}| \to +\infty$ (cf. [7]). Existence and uniqueness results of this problem can be found in [8] and integral representations in [9]. When β is purely imaginary, and such that $\mathrm{Im}\,(\beta) < 0$, the boundary is said to have a non-absorbing property since it allows the propagation of surface waves. In such case, the scattered field has a different behavior near the surface. In [10], an equivalent Sommerfeld-type radiation condition is given explicitly for the scattered field and also existence and uniqueness results are proven for the solutions. In [11], an integral representation is presented and a boundary element formulation is defined over the local perturbation. A more detailed description can be found likewise in [12].

The main problem when dealing with such an integral representation is that the Green's function, which is given in terms of an integral form, needs to be approximated accurately. When considering the non-absorbing case, certain values of the involved parameters make the numerical approximation of the associated Green's function unstable, generating several difficulties in the implementation of the integral representation (cf. [12]). In [11] an Inverse Fast Fourier Transform (IFFT) numerical approximation for the non-absorbing case is proposed. The method is numerically stable and the authors validate it by considering several numerical experiments. The principal disadvantage of the IFFT method is the large number of samples required to obtain an accurate approximation for the Fourier transform, making it an inefficient approximation when a large number of Green's function evaluations is required, for instance, when considering its integral representation or when approximating it by the Boundary Element Method (BEM). In [12], an alternative approximation is proposed, which considers different approaches depending on the far and near field behaviors of the Green's function, and utilizes integral identities to treat singularities and numerical stability problems. Faster approximations than the IFFT approach are possible to obtain with the given representations, however at a trade-off in accuracy. Also, the treatment of several expressions is required for its implementation, making it difficult in practice. More recently, in [13] a hybrid method between the Sommerfeld integral and the method of images is proposed, which is claimed to be efficient numerically, however, the non-absorbing case is not treated therein.

The main contribution of this work is the development of a novel and equivalent representation for the Green's function related to the Helmholtz impedance problem in a half-plane, allowing the propagation of surface waves into infinity. This novel representation is numerically stable and has several advantages. On one hand, the involved integral terms are defined over bounded intervals. Such domains depend only on distances in terms of the source and observation points, which has a considerable advantage in the BEM implementation. On the other hand, the bounded nature of said integral terms makes it possible to estimate them by using any well known quadrature rule or numerical method for integrals defined over bounded domains. The equivalent representation can be easily extended to other impedance cases, for instance, to absorbing boundaries.

The remainder of this paper is organized as follows. First we present the direct scattering problem due to a local perturbation of the impedance half-plane. We provide also the integral representation (in terms of the Green's function) and the weak boundary formulation that is satisfied by the outgoing scattered field. Second, we describe the Green's function associated with the impedance problem. Third, we introduce the equivalent representation for the non-absorbing case, giving an extended and detailed explanation of its deduction. We also provide explicit formulas for the computations of the partial derivatives and we discuss the extension to general impedance-type problems. Fourth, we perform numerical experiments validating the accuracy of the proposed approximation. Finally, we conclude and discuss potential future lines of work.

2. The locally perturbed half-plane problem

Let $\mathbb{R}^2_+ := \{\mathbf{x} = (x_1\,,\, x_2\,) \in \mathbb{R}^2 \,:\, x_2 > 0\}$ be the upper half-plane, and denote by $\Gamma_+ := \partial\mathbb{R}^2_+ = \{\mathbf{x} = (x_1\,,\, x_2\,) \in \mathbb{R}^2 \,:\, x_2 = 0\}$ its (infinite) boundary. Define $\Gamma_\infty := \{(x_1, x_2) \in \Gamma_+ \,:\, |x_1| > 1\}$ and let Γ_p be any curve contained in $\mathbb{R}^2_+$ connecting Γ_∞, in such a manner that $\Gamma = \Gamma_p \cup \Gamma_\infty$ corresponds to the boundary of a locally perturbed half-plane, denoted by $\Omega \subset \mathbb{R}^2_+$. Finally, denote by $\mathbf{n}$ the outer normal to Ω (see Fig. 1).

We look for time-harmonic solutions of the scalar acoustic wave equation, i.e. solutions of the form:

$$v(\mathbf{x}, t\,) = \mathrm{Re}\left(u_T(\mathbf{x})\, e^{-i\omega t}\right), \tag{2}$$

where u_T satisfies:

$$\Delta u_T + \kappa^2\, u_T = 0, \ \text{in}\ \Omega, \tag{3}$$

with $\kappa = \omega/c$ the wave number (where c denotes the sound speed), together with the impedance boundary condition:

$$\gamma_z(u_T) = 0, \ \text{on}\ \Gamma, \tag{4}$$

where $\gamma_z(\cdot)$ denotes the impedance trace operator:

$$\gamma_z(u) := -\partial_n u + z\, u, \ \text{on}\ \Gamma, \tag{5}$$

with ∂_n denoting the partial derivative in the exterior normal direction over Γ, and $z > 0$ being the impedance constant.

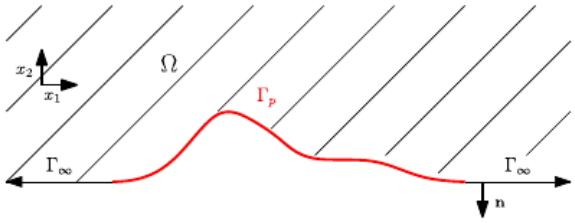

Fig. 1. The locally perturbed half-plane Ω.

We split $u_T = u_i + u$ with u_i being a known incident field satisfying the homogeneous Helmholtz equation (3) in $\mathbb{R}^2_+$ (e.g., an incident plus a reflected plane wave or a surface wave), together with the homogeneous boundary condition (4) over the unperturbed boundary Γ_+, and u being the unknown scattered field satisfying:

$$\begin{cases} \Delta u + \kappa^2 u = 0, & \text{in } \Omega, \\ \gamma_z(u) = -\gamma_z(u_i) := f, & \text{on } \Gamma, \\ \text{Radiation condition (7)}, \end{cases} \tag{6}$$

where, due to the presence of surface waves (see (11)), the outgoing radiation condition for u differs from the standard Sommerfeld radiation condition (cf. [7]) and, for a given $\alpha \in (0, \pi/2)$, is given by (cf. [10]):

$$\begin{cases} |\partial_r u - i\kappa u| < O(r^{\alpha-1}), & \text{if } x_2 > r^\alpha, \\ \left|\partial_r u - i\sqrt{\kappa^2 + z^2} u\right| < O(r^{\alpha-1}), & \text{if } 0 \le x_2 \le r^\alpha, \end{cases} \tag{7}$$

with ∂_r denoting the partial derivative with respect to $r = \sqrt{x_1^2 + x_2^2}$.

As incident field, we can consider two different kinds of wave fields, which do not satisfy the outgoing radiation condition (7):

(i) The plane (volume) wave field:

$$u_i(x_1, x_2) = u_{\text{inc}}(x_1, x_2) + u_{\text{ref}}(x_1, x_2), \tag{8}$$

where u_{inc} is a given standard incident plane (volume) wave of the form:

$$u_{\text{inc}}(x_1, x_2) = A\, e^{i\kappa(x_1 \cos\beta + x_2 \sin\beta)}, \text{ with } A \in \mathbb{C}, \tag{9}$$

and u_{ref} corresponds to its natural plane wave reflection due to the unperturbed boundary Γ_+:

$$u_{\text{ref}}(x_1, x_2) = A\, \frac{\kappa \sin\beta - iz}{\kappa \sin\beta + iz}\, e^{i\kappa(x_1 \cos\beta - x_2 \sin\beta)}. \tag{10}$$

(ii) The (plane) surface wave:

$$u_i(x_1, x_2) = A\, e^{-zx_2} e^{\pm i\sqrt{z^2+\kappa^2} x_1}, \text{ with } A \in \mathbb{C}. \tag{11}$$

This kind of wave is known as a surface wave since it decreases exponentially in the vertical direction x_2 and is oscillatory in the horizontal direction x_1.

Remark 1. If u_i is given either by (8) or (11), it holds that

$$\gamma_z(u_i) = 0 \text{ if } \mathbf{x} \in \Gamma_+, \text{ implying that } \gamma_z(u_i) = 0 \text{ over } \Gamma_\infty. \tag{12}$$

2.1. Integral representation and boundary variational formulation

For $\mathbf{x} \in \Omega$ and $f \in L^2(\Gamma)$ such that $\operatorname{supp} f \subset \Gamma_p$, the solution of problem (6) admits the following integral representation (cf. [11]):

$$u(\mathbf{x}) = \int_{\Gamma_p} \left(\partial_{n_\mathbf{y}} g(\mathbf{x}, \mathbf{y}) - z\, g(\mathbf{x}, \mathbf{y})\right) u(\mathbf{y})\, d\Gamma(\mathbf{y}) + \int_{\Gamma_p} f(\mathbf{y})\, g(\mathbf{x}, \mathbf{y})\, d\Gamma(\mathbf{y}), \tag{13}$$

where g denotes the associated Green's function (see Section 3). By extending by zero towards the complementary domain $\Omega^c := \mathbb{R}^2_+ \setminus \overline{\Omega}$ and by defining an adequate transmission problem, we obtain the following integral equation (for $\mathbf{x} \in \Gamma_p$):

$$\frac{u(\mathbf{x})}{2} = \int_{\Gamma_p} \left(\partial_{n_\mathbf{y}} g(\mathbf{x}, \mathbf{y}) - z\, g(\mathbf{x}, \mathbf{y})\right) u(\mathbf{y})\, d\Gamma(\mathbf{y}) + \int_{\Gamma_p} f(\mathbf{y})\, g(\mathbf{x}, \mathbf{y})\, d\Gamma(\mathbf{y}). \tag{14}$$

From (13) and (14) we obtain the following weak boundary variational formulation:

$$\text{Find } u \in H^{1/2}(\Gamma_p) \text{ such that } b(u,\phi) = l(\phi), \text{ for all } \phi \in H^{1/2}(\Gamma_p), \tag{15}$$

with

$$\begin{aligned} b(u,\phi) = & \int_{\Gamma_p}\int_{\Gamma_p} \left(\partial_{n_{\mathbf{y}}} g(\mathbf{x},\mathbf{y}) - z\, g(\mathbf{x},\mathbf{y})\right) u(\mathbf{y})\, \overline{\phi(\mathbf{x})}\, d\Gamma(\mathbf{y})\, d\Gamma(\mathbf{x}) \\ & - \frac{1}{2}\int_{\Gamma_p} u(\mathbf{x})\, \overline{\phi(\mathbf{x})}\, d\Gamma(\mathbf{x}), \end{aligned} \tag{16}$$

$$l(\phi) = -\int_{\Gamma_p}\int_{\Gamma_p} g(\mathbf{x},\mathbf{y}) f(\mathbf{y})\, \overline{\phi(\mathbf{x})}\, d\Gamma(\mathbf{y})\, d\Gamma(\mathbf{x}). \tag{17}$$

Remark 2. For a given κ, there exists at least a numerable set of values for z for which the solution of the formulation (15) is not unique. An extended and detailed study concerning uniqueness results and the numerical implementation of the integral representation can be found in [12].

3. The Green's function

We consider the unperturbed half-plane $\mathbb{R}^2_+$. For a given and fixed source point $\mathbf{x} = (x_1, x_2) \in \mathbb{R}^2_+$, the associated Green's function $g(\mathbf{x}, \cdot)$ satisfies the problem (recall that $-\partial_{n_{\mathbf{y}}} = \partial_{y_2}$ over Γ_+):

$$\begin{cases} \Delta_{\mathbf{y}} g(\mathbf{x},\mathbf{y}) + \kappa^2\, g(\mathbf{x},\mathbf{y}) = \delta_{\mathbf{x}}(\mathbf{y}) & \text{in } \mathbb{R}^2_+, \\ \partial_{y_2} g(\mathbf{x},\mathbf{y}) + z\, g(\mathbf{x},\mathbf{y}) = 0 \qquad \text{on } \Gamma_+, \\ + \text{Radiation condition (7) in terms of } \mathbf{y}. \end{cases} \tag{18}$$

The standard procedure to obtain the solution of the previous problem consists in first considering a Fourier transform in the y_1 variable, obtaining a spectral ordinary differential equation (ODE) problem in terms of the y_2 variable, then to solve analytically the spectral ODE problem, and finally to recover the spatial solution through an inverse Fourier transform. However, when allowing the presence of surface waves, the spectral solution presents singularities (simple poles) at the spectral points $\pm\xi_p$, with:

$$\xi_p := \sqrt{\kappa^2 + z^2}. \tag{19}$$

In fact, the spectral Fourier transform of the Green's function is given by (cf. [10]):

$$\begin{aligned} \widehat{g}(\mathbf{x},\xi,y_2) = & \frac{1}{\sqrt{8\pi}} \frac{z+\sqrt{\xi^2-\kappa^2}}{z-\sqrt{\xi^2+\kappa^2}} \frac{e^{-\sqrt{\xi^2-\kappa^2}(y_2+x_2)}}{\sqrt{\xi^2-\kappa^2}} \\ & - \frac{1}{\sqrt{8\pi}} \frac{e^{-\sqrt{\xi^2-\kappa^2}|y_2-x_2|}}{\sqrt{\xi^2-\kappa^2}}. \end{aligned} \tag{20}$$

To recover the spatial solution, we apply the limiting absorption principle by considering, for the wave number κ, the small perturbation:

$$\kappa_\varepsilon = \kappa + i\,\varepsilon, \text{ with } \varepsilon > 0. \tag{21}$$

The spatial Green's function is then represented as the limit:

$$g(\mathbf{x},\mathbf{y}) = \lim_{\varepsilon\to 0^+} \frac{1}{\sqrt{2\pi}} \int_{-\infty}^{+\infty} \widehat{g}_\varepsilon(\mathbf{x},\xi,y_2)\, e^{i\xi(y_1-x_1)}\, d\xi, \tag{22}$$

where $\widehat{g}_\varepsilon$ denotes the spectral function $\widehat{g}$ after changing κ by κ_ε.

Remark 3. In definition (22), the complex meaning of the square root value $\sqrt{\xi^2-\kappa_\varepsilon^2}$ is implicitly defined, which is required when establishing the radiation condition (7). For a sufficiently small ε, the complex paths are selected in such a manner that

$$\begin{cases} \sqrt{\xi^2-\kappa_\varepsilon^2} = -i\sqrt{\kappa^2-\xi^2}, & \text{when } \varepsilon \to 0^+ \text{ and } |\xi| \le \kappa, \\ \quad \text{Re}\left(\sqrt{\xi^2-\kappa_\varepsilon^2}\right) > 0, & \text{when } \varepsilon \to 0^+ \text{ and } |\xi| > \kappa. \end{cases} \tag{23}$$

The same root definition will be kept throughout this work.

4. The equivalent Green's function

From expression (13) it is clear that, to obtain an accurate approximation for the solution, a stable and robust approximation of the Green's function g as well as for its gradient ∇g is required. In this section, we present the equivalent representation for the Green's function (22) that is given explicitly in the following main theorem:

Theorem 1. *Let $\kappa, z \in \mathbb{R}_+$. The Green's function (22) can be written equivalently as:*

$$g(\mathbf{x},\mathbf{y}) = g_N(\mathbf{x},\mathbf{y}) + z\left(g_{I_1} + g_{I_2} + g_S + g_R\right)(\mathbf{v}), \tag{24}$$

with

$$g_N(\mathbf{x},\mathbf{y}) = -\frac{i}{4}\left(H_0^{(1)}(\kappa|\mathbf{y}-\mathbf{x}|) + H_0^{(1)}\left(\kappa|\mathbf{y}-\bar{\mathbf{x}}|\right)\right), \tag{25}$$

$$g_{I_1}(\mathbf{v}) = -\frac{iz}{2\xi_p}\, e^{-zv_2}\int_0^{|v_1|} H_0^{(1)}(\kappa\lambda)\,\sin\left(\xi_p(\lambda-|v_1|)\right)\,d\lambda, \tag{26}$$

$$g_{I_2}(\mathbf{v}) = \frac{i}{2}\int_0^{v_2} e^{(\lambda-v_2)z} H_0^{(1)}\left(\kappa\sqrt{v_1^2+\lambda^2}\right)\,d\lambda, \tag{27}$$

$$g_S(\mathbf{v}) = -\frac{i}{\xi_p}\, e^{-zv_2} e^{i\xi_p|v_1|}, \tag{28}$$

$$\begin{aligned} g_R(\mathbf{v}) = &-\frac{i}{\xi_p\pi}\, e^{-zv_2}\cos(\xi_p v_1)\left(\tan^{-1}\left(\frac{iz}{\xi_p}\right) - \frac{\pi}{2}\right) \\ &-\frac{1}{2\xi_p} e^{-zv_2}\sin(\xi_p|v_1|), \end{aligned} \tag{29}$$

where $H_0^{(1)}$ denotes the Hankel function of the first type of order zero (cf. [14]), $\bar{\mathbf{x}} = (x_1, -x_2)$ is the image point of $\mathbf{x}$ in the lower half-plane, and

$$\mathbf{v} = (v_1, v_2) := (y_1 - x_1, y_2 + x_2). \tag{30}$$

Proof. It is direct from Propositions 1, 2, and 6, given below.

Remark 4. $g_N(\mathbf{x},\mathbf{y})$ defined in (25) is the Green's function associated with a homogeneous Neumann-type boundary condition over Γ_+, i.e., the Green's function satisfying problem (18) for $z = 0$ (cf. [15]). Its Fourier integral representation is given by:

$$\begin{aligned} g_N(\mathbf{x},\mathbf{y}) = &-\frac{1}{4\pi}\int_{-\infty}^{+\infty} \frac{e^{-\sqrt{\xi^2-\kappa^2}|y_2-x_2|}}{\sqrt{\xi^2-\kappa^2}} e^{i\xi(y_1-x_1)}\,d\xi \\ &-\frac{1}{4\pi}\int_{-\infty}^{+\infty} \frac{e^{-\sqrt{\xi^2-\kappa^2}(y_2+x_2)}}{\sqrt{\xi^2-\kappa^2}} e^{i\xi(y_1-x_1)}\,d\xi. \end{aligned} \tag{31}$$

The remaining part of this section is dedicated to prove the results required to obtain the equivalent representation (24).

One of the principal complexities of the integral representation (22) is that it depends on the perturbation $\varepsilon > 0$, giving an additional error in the approximation. We start by removing such dependency by proving the following proposition:

Proposition 1. *The Green's function (22) can be equivalently written as:*

$$g(\mathbf{x},\mathbf{y}) = g_N(\mathbf{x},\mathbf{y}) + z\left(g_{int}(\mathbf{v}) + g_S^{Re}(\mathbf{v})\right), \tag{32}$$

where $g_N(\mathbf{x},\mathbf{y})$ is the Green's function defined in (25),

$$g_{int}(\mathbf{v}) = -\frac{1}{2\pi}\int_{-\infty}^{+\infty}\left(\frac{e^{-\sqrt{\xi^2-\kappa^2}v_2}}{(\sqrt{\xi^2-\kappa^2}-z)\sqrt{\xi^2-\kappa^2}} - \frac{2e^{-zv_2}}{\xi^2-\xi_p^2}\right) e^{i\xi v_1}\,d\xi, \tag{33}$$

and

$$g_S^{Re}(\mathbf{v}) = \frac{1}{\xi_p} e^{-zv_2}\sin(\xi_p|v_1|). \tag{34}$$

Proof. First note that $\widehat{g}(\mathbf{x}, \xi, y_2)$ (defined in (20)) can be written as:

$$\begin{aligned}\widehat{g}(\mathbf{x}, \xi, y_2) &= \frac{1}{\sqrt{8\pi}} \frac{2z - z + \sqrt{\xi^2 - \kappa^2}}{z - \sqrt{\xi^2 + \kappa^2}} \frac{e^{-\sqrt{\xi^2-\kappa^2}(y_2+x_2)}}{\sqrt{\xi^2 - \kappa^2}} \\ &\quad - \frac{1}{\sqrt{8\pi}} \frac{e^{-\sqrt{\xi^2-\kappa^2}|y_2-x_2|}}{\sqrt{\xi^2 - \kappa^2}} \\ &= \frac{2z}{\sqrt{8\pi}} \frac{e^{-\sqrt{\xi^2-\kappa^2}(y_2+x_2)}}{(z - \sqrt{\xi^2 + \kappa^2})\sqrt{\xi^2 - \kappa^2}} \\ &\quad - \frac{1}{\sqrt{8\pi}} \frac{e^{-\sqrt{\xi^2-\kappa^2}(y_2+x_2)}}{\sqrt{\xi^2 - \kappa^2}} - \frac{1}{\sqrt{8\pi}} \frac{e^{-\sqrt{\xi^2-\kappa^2}|y_2-x_2|}}{\sqrt{\xi^2 - \kappa^2}}.\end{aligned}$$

On the other hand, the singularity ξ_p (defined in (19)) satisfies $\xi_p > \kappa$. Thus, the representation (22) can be written equivalently as (see Remark 4):

$$\begin{aligned}g(\mathbf{x}, \mathbf{y}) &= -\frac{1}{4\pi} \int_{-\infty}^{+\infty} \frac{e^{-\sqrt{\xi^2-\kappa^2}|y_2-x_2|}}{\sqrt{\xi^2 - \kappa^2}} e^{i\xi(y_1-x_1)}\, d\xi \\ &\quad - \frac{1}{4\pi} \int_{-\infty}^{+\infty} \frac{e^{-\sqrt{\xi^2-\kappa^2}(y_2+x_2)}}{\sqrt{\xi^2 - \kappa^2}} e^{i\xi(y_1-x_1)} d\xi \\ &\quad + \lim_{\varepsilon\to 0^+} \frac{z}{2\pi} \int_{-\infty}^{+\infty} \frac{e^{-\sqrt{\xi^2-\kappa_\varepsilon^2}(y_2+x_2)} e^{i\xi(y_1-x_1)}}{(z - \sqrt{\xi^2 - \kappa_\epsilon^2})\sqrt{\xi^2 - \kappa_\varepsilon^2}} d\xi \\ &=: g_N(\mathbf{x}, \mathbf{y}) + z \lim_{\varepsilon\to 0^+} g_{\text{int},\varepsilon}(\mathbf{x}, \mathbf{y}). \end{aligned} \tag{35}$$

Since $\sqrt{\xi^2 - \kappa^2} - z \approx \frac{\xi_p}{z}(\xi - \xi_p)$ near ξ_p, we can remove the singularity in (35) by using the following equality:

$$\frac{1}{\pi} e^{-zv_2} \text{ p.v.} \int_{-\infty}^{\infty} \frac{e^{i\xi v_1}}{\xi^2 - \xi_p^2}\, d\xi = -\frac{1}{\xi_p} e^{-zv_2} \sin(\xi_p|v_1|), \tag{36}$$

where p.v. denotes the Cauchy principal value (cf. [16]). Therefore, we obtain the following equivalent expression for the limit term at the right-hand side of (35):

$$\lim_{\varepsilon\to 0} g_{\text{int},\varepsilon}(\mathbf{v}) = g_{\text{int}}(\mathbf{v}) + g_S^{\text{Re}}(\mathbf{v}), \tag{37}$$

which completes the proof.

Remark 5. The term g_S^{Re} in the previous representation corresponds to the real part of the asymptotic surface wave behavior of the Green's function (cf. [10]). Another important observation is that the Green's function satisfying the homogeneous Neumann boundary condition at Γ is naturally recovered when $z \to 0^+$.

Remark 6. The value of $g_{\text{int}}(\mathbf{v})$ in (33) is finite for all $v_1 \in \mathbb{R}$ and $v_2 \geq 0$. Thus, it can be estimated by any quadrature rule for indefinite integrals. However, for certain values of κ and z (in particular when $\frac{\kappa}{z} \ll 1$), the representation (33) could become unstable for small values of $|v_1|$ and v_2, requiring to call upon expensive and complex techniques to obtain accurate approximations (cf. [12]). The complexity increases when computing also $\partial_{y_1} g_{\text{int}}(\mathbf{v})$, since it is not integrable when $v_1 = 0$. In fact, the integrand behaves as $C/|\xi|$, when $|\xi| \to +\infty$. Finally, since a quadrature rule for infinite intervals is required, the total time consumed in the implementation of the Boundary Element Method (BEM) implementation increases considerably when considering large partitions of the boundary.

Remark 7. Instead of using the identity (35), the Green's function (22) can be written as:

$$\begin{aligned}g(\mathbf{x}, \mathbf{y}) &= -\frac{1}{4\pi} \int_{-\infty}^{+\infty} \frac{e^{-\sqrt{\xi^2-\kappa^2}|y_2-x_2|}}{\sqrt{\xi^2 - \kappa^2}} e^{i\xi(y_1-x_1)}\, d\xi \\ &\quad + \frac{1}{4\pi} \int_{-\infty}^{+\infty} \frac{e^{-\sqrt{\xi^2-\kappa^2}(y_2+x_2)}}{\sqrt{\xi^2 - \kappa^2}} e^{i\xi(y_1-x_1)} d\xi\end{aligned}$$

$$+ \lim_{\varepsilon\to 0^+} \frac{1}{2\pi}\int_{-\infty}^{+\infty} \frac{e^{-\sqrt{\xi^2-\kappa_\varepsilon^2}(y_2+x_2)}\, e^{i\xi(y_1-x_1)}}{z-\sqrt{\xi^2-\kappa_\epsilon^2}}\, d\xi$$
$$=: g_D(\mathbf{x},\mathbf{y}) + \lim_{\varepsilon\to 0^+} \widetilde{g}_{\text{int},\varepsilon}(\mathbf{x},\mathbf{y}), \tag{38}$$

where $g_D(\mathbf{x},\mathbf{x})$ corresponds to the solution of problem (18) for the Dirichlet boundary condition case, i.e., for the solution for $z \to +\infty$. The principal problem is that the integrand in $\widetilde{g}_{\text{int},\varepsilon}(\mathbf{x},\mathbf{y})$ is not integrable in the subinterval $|\xi| > \xi_p$, when $v_1 = v_2 = 0$. In fact, it behaves as $C/|\xi|$. This in practice leads to an additional instability, implying the necessity of the use of complex and inaccurate approximations to deal with the non-integrability (cf. [12]).

Next, an equivalent representation for the integral term (33) is derived. The following proposition holds true:

Proposition 2. *For all $v_1 \in \mathbb{R}$, the integral expression (33) can be written as:*

$$g_{int}(\mathbf{v}) = \frac{i}{2}\int_0^{v_2} e^{(\lambda-v_2)z} H_0^{(1)}\left(\sqrt{v_1^2+\lambda^2}\right) d\lambda + e^{-zv_2} g_{int}(v_1,0). \tag{39}$$

Proof. We first note that

$$\partial_{y_2}\left(\frac{2e^{-zv_2}}{\xi^2-\xi_p^2}\right) = -z\,\frac{2e^{-zv_2}}{\xi^2-\xi_p^2}. \tag{40}$$

On the other hand, it holds that

$$\partial_{y_2}\left(\frac{e^{-\sqrt{\xi^2-\kappa^2}v_2}}{(\sqrt{\xi^2-\kappa^2}-z)\sqrt{\xi^2-\kappa^2}}\right) = -\frac{e^{-\sqrt{\xi^2-\kappa^2}v_2}}{\sqrt{\xi^2-\kappa^2}-z}. \tag{41}$$

Using the following identity:

$$\frac{1}{\sqrt{\xi^2-\kappa^2}-z} = \frac{z}{(\sqrt{\xi^2-\kappa^2}-z)\sqrt{\xi^2-\kappa^2}} + \frac{1}{\sqrt{\xi^2-\kappa^2}}, \tag{42}$$

we conclude that, for a fixed value of $v_1 \in \mathbb{R}$, the function:

$$u_1(\lambda) := g_{\text{int}}(v_1,\lambda) : (0,v_2) \to \mathbb{R}, \tag{43}$$

satisfies the following Ordinary Differential Equation (ODE):

$$\partial_{y_2} u_1(\lambda) + z\,u_1(\lambda) = \frac{i}{2} H_0^{(1)}\left(\kappa\sqrt{v_1^2+\lambda^2}\right), \text{ with } \lambda \in (0,v_2). \tag{44}$$

The proof is then completed by observing that (39) is the unique solution of problem (44) that satisfies the initial condition $u_1(0) = g_{\text{int}}(v_1,0)$.

In what follows, we derive an equivalent expression for $g_{\text{int}}(v_1,0)$. In a similar way, we derive it as a solution of an ODE problem in terms of the variable v_1. To do so, we start by proving the following proposition:

Proposition 3. *The function $u_2(\lambda) := g_{int}(\lambda,0) : I(v_1) \to \mathbb{R}$ satisfies the following differential equation:*

$$\partial_{y_1}^2 u_2(\lambda) + \xi_p^2\, u_2(\lambda) = z\frac{i}{2} H_0^{(1)}(\kappa|\lambda|), \text{ with } \lambda \in I(v_1) \tag{45}$$

where $\xi_p^2 = \kappa^2 + z^2$ is the square power of the singularity points defined in (19), and

$$I(v_1) = \begin{cases} (0,v_1) & \text{if} \quad v_1 > 0, \\ (v_1,0) & \text{if} \quad v_1 < 0. \end{cases} \tag{46}$$

Proof. As a consequence of (44), considering the partial derivative of (39) with respect to y_2 twice, and thereafter the limit when $v_2 \to 0^+$, we obtain:

$$\begin{aligned}\partial_{y_2}^2 g_{int}(v_1,0) &= z^2 g_{\text{int}}(v_1,0) - z\frac{i}{2}H_0^{(1)}(\kappa|v_1|) \\ &\quad - i\kappa \lim_{v_2\to 0^+} \frac{H_1^{(1)}(\kappa|\mathbf{v}|)}{|\mathbf{v}|}\, v_2 \\ &= z^2 g_{\text{int}}(v_1,0) - z\frac{i}{2}H_0^{(1)}(\kappa|v_1|).\end{aligned} \tag{47}$$

Due to linearity, it is easy to check that g_{int} satisfies the homogeneous Helmholtz equation (18). In fact, we note that the equality with the delta distribution is already satisfied by the Neumann Green's function g_N (see (25)). Therefore, we have that $g_{\text{int}}(v_1, 0)$ must satisfy (45), which completes the proof.

To obtain a unique representation for $g_{\text{int}}(v_1, 0)$ from (45), we need to deduce two additional conditions at $v_1 = 0$. Prior to their definition, we prove the following propositions:

Proposition 4. *For $v_1, \neq 0$ and $v_2 > 0$, the integral function:*

$$\partial_{y_1} g_{I_2}(\mathbf{v}) := -\frac{i\kappa}{2} \int_0^{v_2} e^{(\lambda - v_2)z} \frac{H_1^{(1)}\left(\kappa\sqrt{v_1^2 + \lambda^2}\right)}{\sqrt{v_1^2 + \lambda^2}} v_1 \, d\lambda, \tag{48}$$

satisfies:

$$\lim_{v_1 \to 0^{\pm}} \partial_{y_1} g_{I_2}(\mathbf{v}) = -\frac{1}{2} e^{-v_2 z} \operatorname{sign}(v_1), \tag{49}$$

with $\operatorname{sign}(\cdot)$ *denoting the sign function.*

Proof. For $\tau \to 0^+$, the following identity holds (cf. [14]):

$$H_1^{(1)}(\tau) = -\frac{2i}{\pi\tau} + O(\tau \log \tau). \tag{50}$$

Thus, we have that

$$\frac{H_1^{(1)}\left(\kappa\sqrt{v_1^2 + \lambda^2}\right)}{\sqrt{v_1^2 + \lambda^2}} v_1 = -\frac{2 v_1 i}{\pi\kappa(v_1^2 + \lambda^2)} + O\left(\kappa\, v_1 \log\left(\kappa\sqrt{v_1^2 + \lambda^2}\right)\right). \tag{51}$$

Then, by using the expression $e^{-v_2 z} \frac{2 v_1 i}{\pi\kappa(v_1^2 + \lambda^2)}$ and adding an ad-hoc zero to the integral (48), we have (when $|v_1| \to 0^+$) that

$$\begin{aligned} \partial_{y_1} g_{I_2} &= -\frac{1}{\pi} e^{-v_2 z} \int_0^{v_2} \frac{v_1}{v_1^2 + \lambda^2} \, d\lambda + O(v_1) \\ &= -\frac{1}{\pi} e^{-v_2 z} \tan^{-1}\left(\frac{v_2}{v_1}\right) + O\left(e^{-v_2 z} v_1\right). \end{aligned} \tag{52}$$

The proof is completed by noting that $\lim_{v_1 \to 0^{\pm}} \tan^{-1}\left(\frac{v_2}{v_1}\right) = \frac{\pi}{2} \operatorname{sign}(v_1)$ when $v_2 > 0$.

Proposition 5. *For $v_1 \in \mathbb{R}$ and $v_2 \geq 0$, $g_{int}(\mathbf{v})$ satisfies:*

(i) $g_{int}(0, 0) = -\frac{i}{\xi_p}\left(\frac{1}{\pi}\tan^{-1}\left(\frac{iz}{\xi_p}\right) - \frac{1}{2}\right)$.

(ii) $\lim_{v_1 \to 0^{\pm}} \partial_{y_1} g_{int}(v_1, 0) = -\frac{1}{2}\operatorname{sign}(v_1)$.

Proof. To prove (i) we note that $g_{\text{int}}(0, 0)$ can be solved analytically. In fact, when using the convention $\sqrt{-\xi_p^2} = -i\sqrt{\xi_p^2} = -i\xi_p$ (see Remark 3), its value is given by:

$$\begin{aligned} g_{\text{int}}(0, 0) &= -\frac{1}{2\pi} \int_{-\infty}^{+\infty} \left(\frac{1}{(\sqrt{\xi^2 - \kappa^2} - z)\sqrt{\xi^2 - \kappa^2}} - \frac{2}{\xi^2 - \xi_p^2} \right) d\xi \\ &= -\frac{1}{\pi} \int_0^{+\infty} \left(\frac{1}{(\sqrt{\xi^2 - \kappa^2} - z)\sqrt{\xi^2 - \kappa^2}} - \frac{2}{\xi^2 - \xi_p^2} \right) d\xi \\ &= -\frac{i}{\pi\xi_p} \lim_{t \to +\infty} \left(\tan^{-1}\left(\frac{tzi}{\sqrt{t^2 - \kappa^2}\xi_p} \right) - \tan^{-1}\left(\frac{ti}{\xi_p} \right) \right) \\ &= -\frac{i}{\xi_p} \left(\frac{1}{\pi}\tan^{-1}\left(\frac{iz}{\xi_p} \right) - \frac{1}{2} \right). \end{aligned} \tag{53}$$

To prove (ii) we first note that the partial derivative with respect to y_1 of the integral representation of g_{int} in (33) is not integrable when $v_1 = 0$. However, from the integral representation (35) of $g(\mathbf{x}, \mathbf{y})$, we can easily conclude that

$$\lim_{v_1 \to 0^{\pm}} \partial_{y_1} g(\mathbf{x}, \mathbf{y}) = 0. \tag{54}$$

Since g_N already satisfies (54), from representation (32) we conclude that

$$\lim_{v_1 \to 0^{\pm}} \partial_{y_1} \left(g_{\text{int}}(\mathbf{v}) + g_S^{\text{Re}}(\mathbf{v}) \right) = 0. \tag{55}$$

The expression for $g_S^{\text{Re}}(\mathbf{v})$ can be computed analytically and is given by:

$$\lim_{v_1 \to 0^{\pm}} \partial_{y_1} g_S^{\text{Re}}(\mathbf{v}) = -\operatorname{sign}(v_1) e^{-z v_2}. \tag{56}$$

On the other hand, (39) implies that

$$\begin{aligned} \lim_{v_1 \to 0^{\pm}} \frac{\partial g_{\text{int}}}{\partial y_1}(\mathbf{v}) = & -\lim_{v_1 \to 0^{\pm}} \frac{i\kappa}{2} \int_0^{v_2} e^{(\lambda - v_2)z} \frac{H_1^{(1)}\left(\sqrt{v_1^2 + \lambda^2}\right)}{\sqrt{v_1^2 + \lambda^2}} v_1 \, d\lambda \\ & + \lim_{v_1 \to 0^{\pm}} e^{-z v_2} \partial_{y_1} g_{\text{int}}(v_1, 0). \end{aligned} \tag{57}$$

From Proposition 4 and relations (55) and (56), we finally conclude that

$$\lim_{v_1 \to 0^{\pm}} \partial_{y_1} g_{\text{int}}(v_1, 0) = -\frac{1}{2} \operatorname{sign}(v_1), \tag{58}$$

which completes the proof.

Now we can prove the following proposition:

Proposition 6. *For $v_1 \in \mathbb{R}$, $g_{int}(v_1, 0)$ can be written as:*

$$\begin{aligned} g_{int}(v_1, 0) = & -z \frac{i}{2\xi_p} \int_0^{|v_1|} H_0^{(1)}(\kappa\lambda) \sin\left(\xi_p(\lambda - |v_1|)\right) d\lambda \\ & - \frac{i}{\xi_p} \left(\frac{1}{\pi} \tan^{-1}\left(\frac{iz}{\xi_p}\right) - \frac{1}{2} \right) \cos(\xi_p v_1) - \frac{1}{2\xi_p} \sin(\xi_p |v_1|). \end{aligned} \tag{59}$$

Proof. The proof is a direct consequence by noting that (59) is the unique solution of the differential problem (45), satisfying the initial conditions (i) and (ii) of Proposition 5.

4.1. Expressions for the derivatives of the Green's function

As mentioned in Section 4, to obtain the boundary integral representation of the locally perturbed half-space problem, it is required to estimate also the gradient of the Green's function. It can be immediately obtained from representation (24), and the following propositions hold true:

Proposition 7. *For the Green's function defined in (24), we have that*

$$\partial_{y_1} g(\mathbf{x}, \mathbf{y}) = \partial_{y_1} g_N(\mathbf{x}, \mathbf{y}) + z \left(\partial_{y_1} g_{I_1} + \partial_{y_1} g_{I_2} + \partial_{y_1} g_S + \partial_{y_1} g_R \right)(\mathbf{v}), \tag{60}$$

with

$$\partial_{y_1} g_N(\mathbf{x}, \mathbf{y}) = \frac{i\kappa(y_1 - x_1)}{4} \left(\frac{H_1^{(1)}(\kappa|\mathbf{y} - \mathbf{x}|)}{|\mathbf{y} - \mathbf{x}|} + \frac{H_1^{(1)}\left(\kappa|\mathbf{y} - \bar{\mathbf{x}}|\right)}{|\mathbf{y} - \bar{\mathbf{x}}|} \right), \tag{61}$$

$$\partial_{y_1} g_{I_1}(\mathbf{x}, \mathbf{y}) = \frac{iz^2}{2} \operatorname{sign}(v_1) e^{-z v_2} \int_0^{|v_1|} H_0^{(1)}(\kappa\lambda) \cos\left(\xi_p(\lambda - |v_1|)\right) d\lambda, \tag{62}$$

$$\partial_{y_1} g_{I_2}(\mathbf{v}) = -\frac{iz\kappa}{2} \int_0^{v_2} e^{(\lambda - v_2)z} \frac{H_1^{(1)}\left(\kappa\sqrt{v_1^2 + \lambda^2}\right)}{\sqrt{v_1^2 + \lambda^2}} v_1 \, d\lambda, \tag{63}$$

$$\partial_{y_1} g_S(\mathbf{v}) = z \operatorname{sign}(v_1) e^{-z v_2} e^{i\xi_p |v_1|}, \tag{64}$$

$$\partial_{y_1} g_R(\mathbf{v}) = \; ize^{-z v_2} \sin(\xi_p v_1) \left(\frac{\tan^{-1}\left(\frac{iz}{\xi_p}\right)}{\pi} - \frac{1}{2} \right) - \operatorname{sign}(v_1) \frac{z}{2} e^{-z v_2} \cos(\xi_p |v_1|). \tag{65}$$

Remark 8. We note that $\partial_{x_1} g(\mathbf{x}, \mathbf{y}) = -\partial_{y_1} g(\mathbf{x}, \mathbf{y})$.

Proposition 8. *For the Green's function defined in (24), we have that*

$$\partial_{y_2} g(\mathbf{x}, \mathbf{y}) = \partial_{y_2} g_N(\mathbf{x}, \mathbf{y}) + z \frac{i}{2} H_0^{(1)}(|\mathbf{v}|) - z^2 \left(g_{I_1} + g_{I_2} + g_S + g_R \right)(\mathbf{v}), \tag{66}$$

with

$$\partial_{y_2} g_N(\mathbf{x}, \mathbf{y}) = \frac{i\kappa}{4} \left(H_1^{(1)}(\kappa|\mathbf{y} - \mathbf{x}|) \frac{y_2 - x_2}{|\mathbf{y} - \mathbf{x}|} + H_1^{(1)}\left(\kappa|\mathbf{y} - \overline{\mathbf{x}}|\right) \frac{y_2 + x_2}{|\mathbf{y} - \overline{\mathbf{x}}|} \right). \tag{67}$$

Remark 9. We note that

$$\partial_{x_2} g_N(\mathbf{x}, \mathbf{y}) = -\frac{i\kappa}{4} \left(H_1^{(1)}(\kappa|\mathbf{y} - \mathbf{x}|) \frac{y_2 - x_2}{|\mathbf{y} - \mathbf{x}|} - H_1^{(1)}(\kappa|\mathbf{y} - \overline{\mathbf{x}}|) \frac{y_2 + x_2}{|\mathbf{y} - \overline{\mathbf{x}}|} \right), \tag{68}$$

while

$$\partial_{x_2} g_T(\mathbf{v}) = \partial_{y_2} g_T(\mathbf{v}), \text{ for } T = I_1, I_2, S, R. \tag{69}$$

4.2. Numerical aspects of the involved integrals

When using the equivalent Green's function (24), the numerical computation is reduced to the approximation of integrals $g_{I_1}(\mathbf{v})$ and $g_{I_2}(\mathbf{v})$ (see (24)). When computing its gradient, it is also required to approximate the integrals $\partial_{y_1} g_{I_1}(\mathbf{v})$ and $\partial_{y_1} g_{I_2}(\mathbf{v})$ (see (60)). For $\eta \to 0^+$, the following asymptotic behavior holds for $H_0^{(1)}(\eta)$ (cf. [14]):

$$H_0^{(1)}(\eta) = C_\gamma + \frac{2i}{\pi} \log(\eta) + O(\eta^2 \log(\eta)). \tag{70}$$

Thus, the integrals $g_{I_1}(\mathbf{v})$, $\partial_{y_1} g_{I_1}(\mathbf{v})$ have a log-type singularity at the origin ($\lambda = 0$) that is integrable. In fact, for a sufficiently small $\varepsilon > 0$, it holds:

$$\int_0^\varepsilon H_0^{(1)}(\kappa\lambda) d\lambda = C_\gamma \varepsilon + \frac{i\kappa}{2\pi} \varepsilon^2 \left(2 \log(\kappa\varepsilon) - 1\right) + O\left(\kappa^2 \varepsilon^3 \log(\kappa\varepsilon)\right). \tag{71}$$

The integral $g_{I_2}(v_1, v_2)$ also has the same type of singularity, but only in the particular case when $v_1 = 0$.

Even if the integral $\partial_{y_1} g_{I_2}(\mathbf{v})$ does not have a singularity when $v_1 \neq 0$, its bad behavior when $|v_1| \to 0^+$ yields inaccurate approximations when evaluating for small values of $|v_1|$. To deal with this issue, we use estimation (52) when $v_2 \neq 0$, and the estimation (ii) of Proposition 5 when $v_2 = 0$.

Fig. 2 shows the contour plots for the real and imaginary parts of the Green's function with the values $\kappa = 3$, $z = 5$, $\mathbf{x} = (0, 1)$ and several values of $\mathbf{y} \in (-5, 5) \times (0, 5)$. Fig. 3 displays the surface plots for the same data. The Green's approximation was obtained by considering the *integral* function of MATLAB.

4.3. Extensions

The equivalent Green's function (24) can be easily generalized to other impedance problems, for instance, when $\kappa \in \mathbb{C}$ or $z \in \mathbb{C}$. However, it is required to take into account the complex meaning of the root $\sqrt{\xi^2 - \kappa^2}$ (see Remark 3). As an example, we consider the absorbing case when $\kappa > 0$ and $z \in \mathbb{C}$ with $\operatorname{Im}((z)) > 0$ (see [8] and [9]). In this case, singularities are not present in the Fourier representation $\widehat{g}(\mathbf{x}, \xi, y_2)$ (see (20)). Thus, the inverse Fourier transform can be taken directly, and it is given by:

$$\begin{aligned} g(\mathbf{x}, \mathbf{y}) &= \frac{1}{\sqrt{2\pi}} \int_{-\infty}^{+\infty} \widehat{g}(\mathbf{x}, \xi, y_2) \, e^{i\xi(y_1 - x_1)} \, d\xi \\ &= g_N(\mathbf{x}, \mathbf{y}) + z \, g_{\text{int}}(\mathbf{v}), \end{aligned} \tag{72}$$

with $g_N(\mathbf{x}, \mathbf{y})$ the Neumann Green's function defined in (25), and

$$g_{\text{int}}(\mathbf{v}) = -\frac{1}{2\pi} \int_{-\infty}^{+\infty} \frac{e^{-\sqrt{\xi^2 - \kappa^2} v_2} \, e^{i\xi v_1}}{(\sqrt{\xi^2 - \kappa^2} - z)\sqrt{\xi^2 - \kappa^2}} \, d\xi. \tag{73}$$

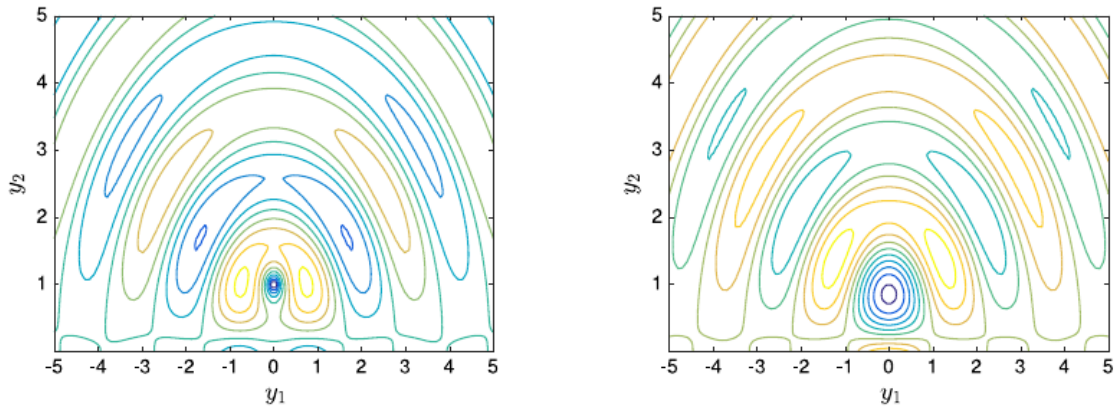

(a) Real part. (b) Imaginary part.

Fig. 2. Contour plots for the Green's function with $\kappa = 3, z = 5$, and a source located at $\mathbf{x} = (0, 1)$.

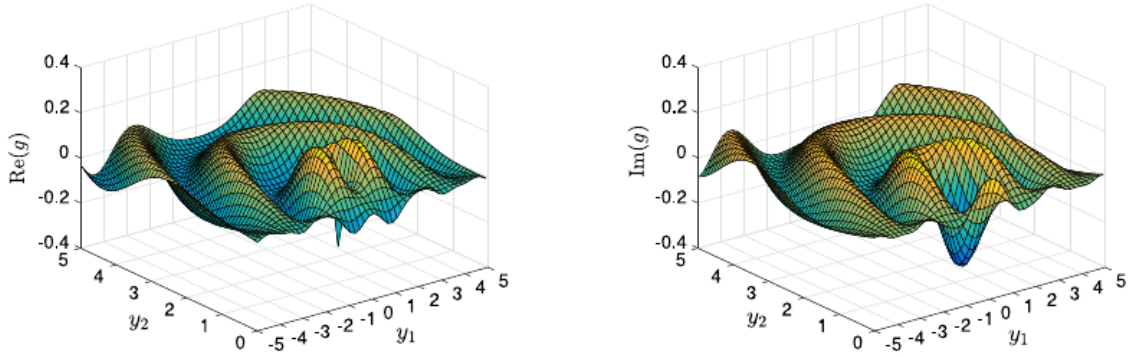

(a) Real part. (b) Imaginary part.

Fig. 3. Surface plots for the Green's function with $\kappa = 3, z = 5$, and a source located at $\mathbf{x} = (0, 1)$.

Using the standard root definition $\sqrt{-\xi_p^2} = i\xi_p$ (see Remark 3), it holds that

$$g_{\text{int}}(0,0) = \frac{i}{2\xi_p}\left(\frac{1}{\pi}\tan^{-1}\left(\frac{z}{i\xi_p}\right) + \frac{1}{2}\right), \text{ with } \xi_p = \sqrt{\kappa^2 + z^2}. \tag{74}$$

On the other hand, it is easy to observe that

$$\lim_{v_1 \to 0^{\pm}} \partial_{y_1} g_{\text{int}}(v_1, 0) = 0. \tag{75}$$

Thus, using an analogous procedure as for Propositions 2 and 6, it is proved that the integral term g_{int} satisfies:

$$g_{\text{int}}(\mathbf{x}, \mathbf{y}) \equiv \left(g_{I_1} + g_{I_2} + g_R\right)(\mathbf{v}), \tag{76}$$

with

$$g_{I_1}(\mathbf{v}) = -\frac{iz}{2\xi_p} e^{-zv_2} \int_0^{|v_1|} H_0^{(1)}(\kappa\lambda) \sin\left(\xi_p(\lambda - |v_1|)\right) d\lambda, \tag{77}$$

$$g_{I_2}(\mathbf{v}) = \frac{i}{2} \int_0^{v_2} e^{(\lambda - v_2)z} H_0^{(1)}\left(\kappa\sqrt{v_1^2 + \lambda^2}\right) d\lambda, \tag{78}$$

$$g_R(\mathbf{v}) = \frac{i}{2\xi_p} \cos(\xi_p v_1) e^{-zv_2} \left(\frac{1}{\pi}\tan^{-1}\left(\frac{z}{i\xi_p}\right) + \frac{1}{2}\right). \tag{79}$$

5. Numerical examples

We consider two numerical experiments. In the first experiment, we obtain an approximation of the Green's function with the Finite Element Method (FEM). The aim is to improve the accuracy and efficiency of the Green's function approximation

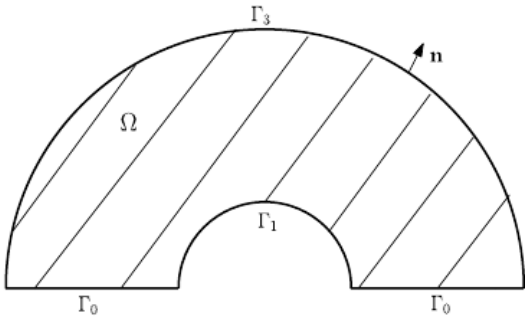

Fig. 4. The half-ring $\Omega \subset \mathbb{R}^2_+$.

(24) in the near field. In the second experiment, we consider an approximation of the Green's function through the Galerkin Boundary Element Method (BEM). In both cases, a good assessment would be to obtain adequate convergence rates in terms of the respective spatial step of each method.

5.1. FEM benchmark

Let Ω be the bounded half-ring domain:

$$\Omega := \left\{ \mathbf{x} \in \mathbb{R}^2_+ \ : \ 1 < \sqrt{x_1^2 + x_2^2} < 3 \right\}, \tag{80}$$

with boundary $\partial\Omega = \Gamma_0 \cup \Gamma_1 \cup \Gamma_3$ as described in Fig. 4, and we approximate the following function (defined in Ω):

$$u_{ex}(\mathbf{x}) := g((0,0), \mathbf{x}), \tag{81}$$

as the solution of the problem:

$$\begin{cases} \text{Find } u \in H^1(\Omega) \text{ such that:} \\ \quad \Delta u + \kappa^2 u = 0, \quad \text{in } \Omega \\ \gamma_z(u) = -\gamma_z(u_{\text{ex}}), \quad \text{over } \partial\Omega. \end{cases} \tag{82}$$

Remark 10. We note that $(0,0) \notin \Omega$, implying that $u_{\text{ex}} \in H^1(\Omega)$. We also note that $\gamma_z(u_{\text{ex}}) = 0$ over Γ_0 (see (12)).

It is well known that the problem (82) has a unique solution (cf. [15]), and thus given by $u(\mathbf{x}) = u_{\text{ex}}(\mathbf{x})$. It can be easily demonstrated that the following Galerkin variational problem is satisfied by the solution of (82):

$$\text{Find } u \in H^1(\Omega) \ : \ a(u,v) = l(v), \ \text{ for all } v \in H^1(\Omega), \tag{83}$$

with

$$a(u,v) = \kappa^2 \int_\Omega u\, \overline{v}\, d\mathbf{x} - \int_\Omega \nabla u \cdot \overline{\nabla v}\, d\mathbf{x} + z \int_{\partial\Omega} u\, \overline{v}\, dS(\mathbf{x}), \tag{84}$$

and

$$l(v) = \int_{\partial\Omega} (\partial_n u_{\text{ex}} - z\, u_{\text{ex}})\, \overline{v}\, dS(\mathbf{x}). \tag{85}$$

By the Fredholm alternative theorem, the problem (83) has a unique solution if κ^2 is not an eigenvalue for the operator $A(u,v) = a(u,v) - \kappa^2 \int_\Omega u\, \overline{v}\, d\mathbf{x}$ (cf. [15]). We discretize (83) by the Galerkin FEM considering several triangular and regular meshes for the domain $\overline{\Omega}$ of size h, obtaining an approximation of u_{ex} denoted by u_h. We use the standard space of continuous and piecewise linear functions $X_h^1 \subset H^1(\Omega)$ for the numerical estimation. We compute the FEM matrix $\left(a(\phi_j, \phi_i)\right)_{i,j}$ by using the FreeFem++ package, while the right hand side and the respective approximated solution u_h by using MATLAB. The estimation of the reference function u_{ex} is obtained by using the *integral* function implemented in MATLAB, where we take into account the numerical aspects described in Section 4.2 for its implementation. We validate the efficiency of the Green's representations (24), (60) and (66) by computing the well known convergence rates:

(i) L^2-relative error:

$$\frac{\|u_h - u_{\text{ex}}\|_{L^2(\Omega)}}{\|u_{\text{ex}}\|_{L^2(\Omega)}} = O(h^2). \tag{86}$$

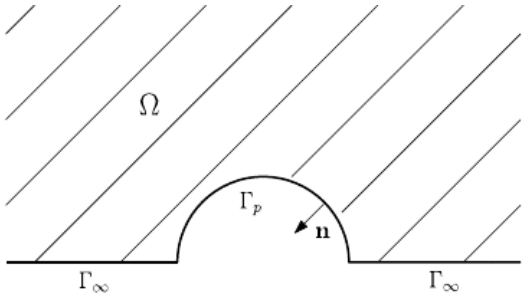

Fig. 5. The unbounded domain $\Omega \subset \mathbb{R}^2_+$.

(ii) H^1-semi norm relative error:

$$\frac{\|\nabla u_h - \nabla u_{\text{ex}}\|_{[L^2(\Omega)]^2}}{\|\nabla u_{\text{ex}}\|_{[L^2(\Omega)]^2}} = O(h). \tag{87}$$

We plot (in log scale) the results obtained for several mesh sizes h, and we compare it with the theoretical convergence rates in terms of h. In Fig. 6(a) we show the L^2-relative error convergence rates obtained by considering a wave number of $k = 0.03$ and several values for the impedance constant z, including the case $z = 0$ which, we recall, is analytic (see (25)). In Fig. 6(b) we show the H^1-semi relative error convergence rates obtained for the same values of k and z considered in Fig. 6(a). In Fig. 7 we repeat the experiments shown in the previous figure, but now considering a wave number of $\kappa = 3$ instead of $\kappa = 0.03$.

In all cases, the theoretical convergence rates (described in (86) and (87)) are reproduced, validating the efficiency of the equivalent Green's function representation.

5.2. BEM benchmark

Let now Ω be the unbounded domain that is exterior to the half-circle centered at the origin with radius equal to one, i.e., the domain:

$$\Omega = \{\mathbf{x} \in \mathbb{R}^2_+ \ : \ x_1^2 + x_2^2 > 1\}, \tag{88}$$

with boundary $\partial\Omega = \Gamma_p \cup \Gamma_\infty$ following the sense described in Fig. 5. As the second experiment, we approximate the exact solution (81) by the BEM formulation (15). We discretize the trace space $H^{1/2}(\Gamma_p)$ by using regular partition of Γ_p of size h, and considering the space of continuous and piecewise linear polynomials defined over Γ_p. We refer to [11] or [12] to see a detailed explanation of the BEM implementation. For the plots, we consider the L^2-relative error for the trace approximation given by:

$$\frac{\|u_{\text{ex}} - u_h\|_{L^2(\Gamma_p)}}{\|u_{\text{ex}}\|_{L^2(\Gamma_p)}}. \tag{89}$$

Fig. 8(a) shows the L^2-relative error slope obtained for $k = 3$. The solution, considering $z = 5$ (the worst behavior in the FEM benchmark), was computed with the *integral* MATLAB function and it was compared with the analytic solution for $z = 0$. Differing with the FEM benchmark, here the theoretical convergence rates suggested in the literature are not obtained. Nevertheless, the same slope (of order h) is obtained for both cases, and we recall that for $z = 0$, the Green's function is analytic. In order to observe its behavior in terms of a standard quadrature, Fig. 8(b) shows the L^2-relative error for $k = 3$ and $z = 5$ by considering variations in the total of the Gaussian quadrature points required in the construction of the BEM matrices. We use the same number of quadrature nodes for all the integrals in all the required evaluations, skipping the singularity at the origin (when it corresponds) by considering the integral departing from $\lambda = 1 \cdot 10^{-8}$ instead of $\lambda = 0$ (see Section 4.2). We compute the error by comparing with the exact solution estimated with the *integral* MATLAB function. It can be observed that even employing a small number of quadrature points, accurate approximations are obtained and the slope obtained in Fig. 8(a) is recovered by just considering 80 quadrature points.

6. Conclusions and future work

We obtained an equivalent representation for the Green's function associated with the Helmholtz problem in a non-absorbing half-plane. The main advantage of the derived equivalent representation is that, differing with the standard Fourier integral representations over $\mathbb{R}$, the integral terms are now bounded. This representation is numerically stable and can be estimated by any well known quadrature formula for integrals defined over bounded intervals. We give the explicit

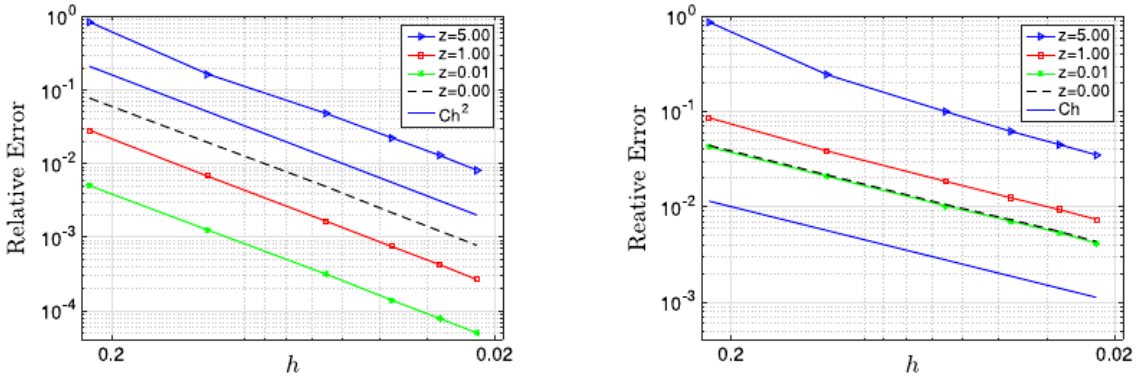

(a) L^2-relative error. (b) H^1-semi relative error.

Fig. 6. Mesh size vs. relative error plots obtained with FEM for $\kappa = 0.03$.

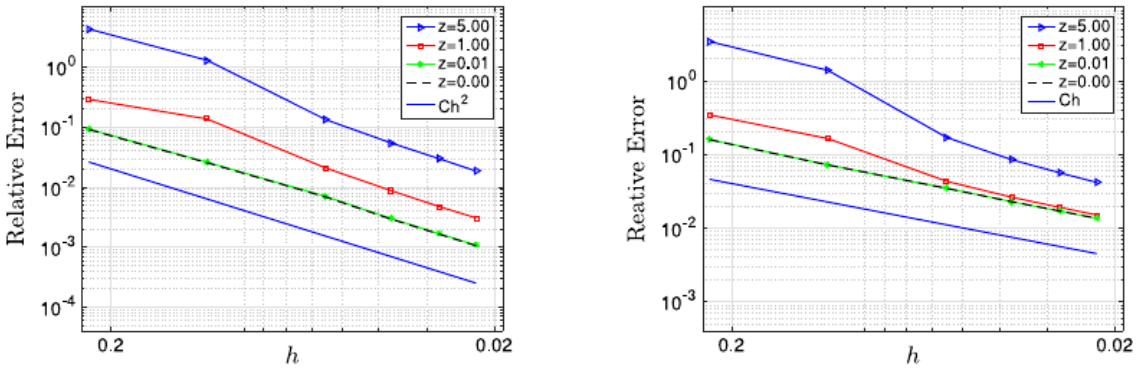

(a) L^2-relative error. (b) H^1-semi relative error.

Fig. 7. Mesh size vs. relative error plots obtained with FEM for $\kappa = 3$.

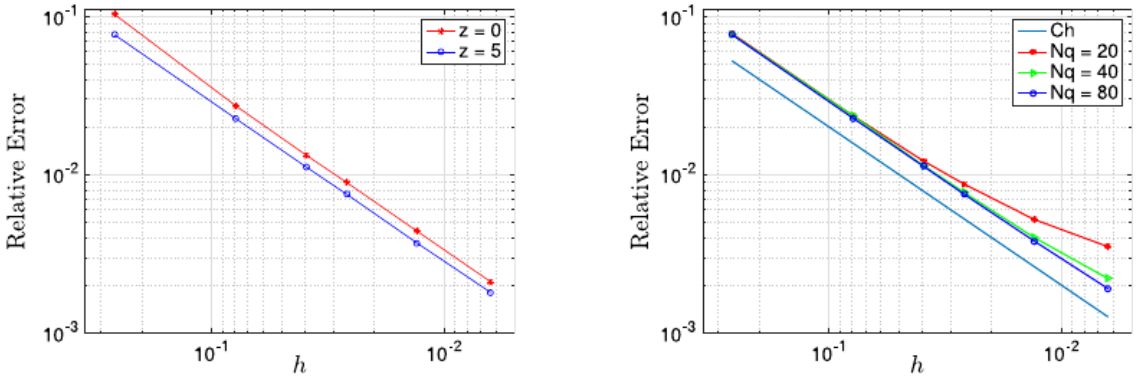

(a) L^2-relative error for $\kappa = 3$. (b) L^2-relative error for $\kappa = 3$ and $z = 5$ considering different quadrature sizes.

Fig. 8. Mesh size vs. L^2 relative error obtained with BEM.

representation and a detailed explanation of its deduction. We give also explicit formulas for the gradient computation. The novel representation can be easily extended to other impedance-type problems. We validate the accuracy of the equivalent representation by considering adequate numerical experiments. With the aim of showing its efficient and simple implementation, we use the standard Gauss–Legendre quadrature rule varying the number of quadrature nodes, as well as the *integral* function of MATLAB to approximate the involved integral values. Fast approximations can be obtained by studying an adequate numerical treatment of the corresponding integrals, however the aim of this work was to present the equivalent representation. The efficient numerical treatment will be considered in future work. An eventual extension to the three-dimensional case will be studied as well.

Acknowledgments

Sergio Rojas acknowledges the support from CONICYT-Chile (grant number: 21120857) through the Ph.D. fellowship program. Additionally, the authors want to thank the anonymous referees and Michael Karkulik for their comments that helped to improve the results of this paper.

References

[1] J.D. Joannopoulos, S.G. Johnson, J.N. Winn, R.D. Meade, Photonic Crystals: Molding the Flow of Light, Princeton university press, 2011.
[2] K. Sakoda, Optical Properties of Photonic Crystals, Vol. 80, Springer Science & Business Media, 2004.
[3] L.-S. Hwang, E.O. Tuck, On the oscillations of harbours of arbitrary shape, J. Fluid Mech. 42 (03) (1970) 447–464.
[4] J.-J. Lee, Wave-induced oscillations in harbours of arbitrary geometry, J. Fluid Mech. 45 (02) (1971) 375–394.
[5] R. Shaw, Long Period Forced Harbor Oscillations, Topics in Ocean Engineering, Gulf Publishing Company, Texas, 1971.
[6] C.L. Mader, Numerical Modeling of Detonations, in: Los Alamos Series in Basic and Applied Sciences, University of California Press, Berkeley, 1979.
[7] A. Sommerfeld, Partial Differential Equations in Physics, Vol. 1, Academic press, 1949.
[8] S. Chandler-Wilde, The impedance boundary value problem for the Helmholtz equation in a half-plane, Math. Methods Appl. Sci. 20 (10) (1997) 813–840.
[9] S.N. Chandler-Wilde, A.T. Peplow, A boundary integral equation formulation for the Helmholtz equation in a locally perturbed half-plane, ZAMM 85 (2) (2005) 79–88.
[10] M. Durán, I. Muga, J.-C. Nédélec, The Helmholtz equation in a locally perturbed half-plane with passive boundary, IMA J. Appl. Math. 71 (6) (2006) 853–876.
[11] M. Durán, R. Hein, J.-C. Nédélec, Computing numerically the Green's function of the half-plane Helmholtz operator with impedance boundary conditions, Numer. Math. 107 (2) (2007) 295–314.
[12] R. Hein Hoernig, Green's functions and integral equations for the Laplace and Helmholtz operators in impedance half-spaces, in: Mathematics, Ecole Polytechnique X, Berlin, 2010.
[13] M. ONeil, L. Greengard, A. Pataki, On the efficient representation of the half-space impedance Green's function for the Helmholtz equation, Wave Motion 51 (1) (2014) 1–13.
[14] M. Abramowitz, I.A. Stegun, Handbook of Mathematical Functions: With Formulas, Graphs, and Mathematical Tables, Vol. 55, Courier Corporation, 1964.
[15] J.-C. Nédélec, Acoustic and Electromagnetic Equations: Integral Representations for Harmonic Problems, Vol. 144, Springer Science & Business Media, 2001.
[16] P. Henrici, Applied and Computational Complex Analysis. Vol. 1, Power Series, Integration, Conformal Mapping, Location of Zeros, Wiley, New York, 1974.